

# Transport of the obstacle arrays driven by chiral active particles with temperature difference

Fan-Hua Meng, Jian-Li Liu and Yu-Ling He<sup>1</sup> 

Guangdong Provincial Key Laboratory of Quantum Engineering and Quantum Materials, School of Physics and Telecommunication Engineering, South China Normal University, 510006 Guangzhou, People's Republic of China

E-mail: [hey1@m.scnu.edu.cn](mailto:hey1@m.scnu.edu.cn)

Received 26 September 2019, revised 3 January 2020

Accepted for publication 27 January 2020

Published 11 February 2020



## Abstract

We perform a numerical investigation of the transport of the obstacle arrays driven by chiral active particles in a two-dimensional periodic channel with temperature difference. The obstacle arrays will move to left (right) only when the average velocity of counterclockwise (clockwise) particles is small. For chiral active particles, the direction of transport is completely determined by the chirality of particles. The average velocity of chiral active particles is a peaked function of angular velocity and initial temperature (or temperature difference). The average velocity of chiral active particles increases linearly with the self-propulsion speed, while it decreases monotonically with the increase of particle number. For obstacle arrays, behaviors of transport become complex, current reversals can be obtained by continuously changing the system parameters (angular velocity, initial temperature, temperature difference, self-propulsion speed and particle number).

Keywords: chiral active particles, temperature difference, obstacle arrays

(Some figures may appear in colour only in the online journal)

## 1. Introduction

Active matter has come under the spotlight of the physical and biophysical research communities and has been studied theoretically and experimentally [1–13, 46]. Different from simple Brownian particles, whose motion is dominated by random thermal fluctuations, active particles, also known as microswimmers, are capable of directed motion. Active particles are

<sup>1</sup> Author to whom any correspondence should be addressed.

able to propel themselves, exhibiting an interplay between random fluctuations and active swimming that drives them into an out-of-equilibrium status [9]. In recent years, there has been a strong growth of research activities in respect of the chiral active matter which is a new species of active matter. Transport behaviors of chiral active matter will perform circular motion (in two dimensions) or helicoidal motion (in three dimensions) rather than swim along straight trajectories [40]. Chiral active particles are asymmetric and exhibit completely different behaviors with achiral particles under asymmetric conditions [14–20]. There are many researches on chiral microswimmers, such as *Escherichia coli* bacteria perform a characteristic chiral motion in the proximity of a surface [21–23], as well as sperm cells [24, 25], and magnetotactic bacteria in rotating external fields [26, 42]. Also, moving down to the nanoscale, molecular-sized chiral microswimmers can be obtained by chemically attaching a chiral molecule with a chiral propeller, e.g. a flagellum [40]. Therefore, in-depth understanding of chiral active matter has fundamental and technological importance.

Recently, a growing number of studies have focused on the transport of particles in complex and crowded environments. The interaction of active particles with obstacles within complex environments plays a key role in a wealth of potential applications [27–37]. Chepizhko and coworker [27] considered a variant of the Vicsek model for self-propelled particles interacting with a heterogeneous environment, which is modeled as a random distribution of either static or diffusive obstacles. Nourhani and coworker [28] studied the drift behavior of chiral self-propelling particles moving on a periodic potential, where they found that particles of different chirality can be separated. Kümmel and coworkers [29] studied the mixtures of active and passive particles. Schirmacher and coworkers [30] investigated magnetotransport with randomly distributed scatterers closing to the field-induced localization transition, which is generated by percolating skipping orbits along the edges of obstacle clusters. Pinçe and coworkers [31] demonstrated that the presence of spatial disorder can alter the long-term dynamics in a colloidal active matter system, making it switch between gathering and dispersal of individuals. Reichhardt and coworkers [32–34] studied the transport of particles in random or periodic obstacle arrays and funnel arrays.

Currently, studies of the interaction of active particles with obstacles mostly focus on the rectification or separation of particles. Obstacles are generally fixed, which can block or facilitate the transport of particles. However, in real systems, not only do obstacles drive particles, but particles can also drive obstacles. Moreover, chiral active particles can be driven by transversal temperature difference [38]. Therefore, it would be interesting to investigate how chiral active particles drive the obstacle arrays in the system with temperature difference. In this work, we study of the obstacle arrays are driven by the moving chiral active particles in a two-dimensional periodic channel with temperature difference. It is found that chiral active particles can drive the obstacle arrays to move along the channel and transport behaviors are different for particles and obstacle arrays. For chiral active particles, the transport direction of particles determined by its chirality. However, for the obstacle arrays, within particular parameter regimes obstacle arrays can travel in a direction which is opposite to the transport direction of particles.

## 2. Model and methods

We consider  $n_a$  chiral active particles (blue disks) interacting with a periodic array of obstacles  $n_o$  (black disks) moving in a two-dimensional periodic channel with temperature difference in the  $y$  direction as shown in figure 1. Chiral active particles are self-propelled with the velocity  $v_0$  and angular velocity  $\Omega$ . Obstacles arrayed with the fixed distance can be driven by the

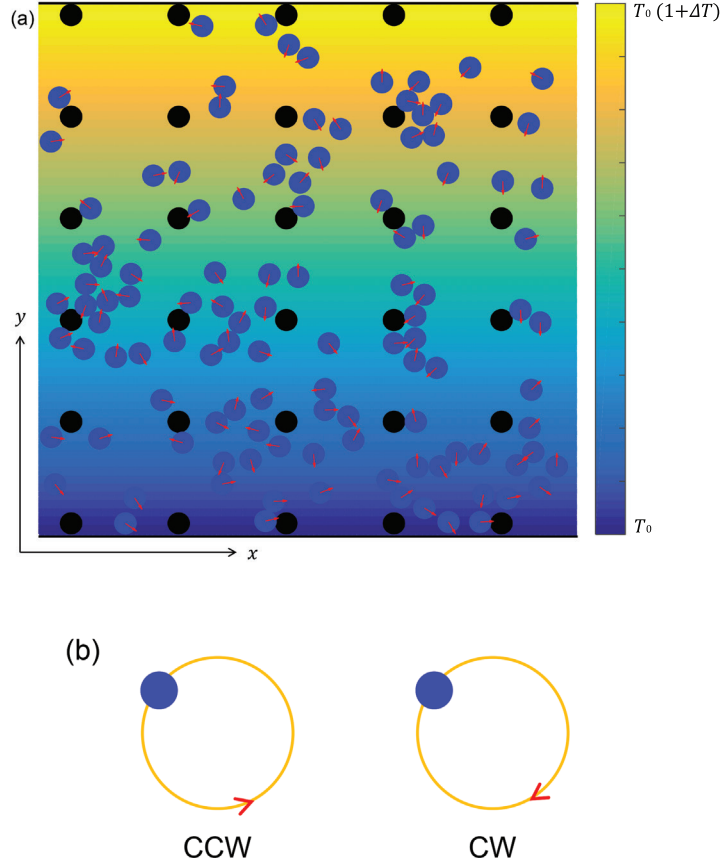


**Figure 1.** (a) Schematic of the obstacle arrays (black disks) are driven by the moving chiral active particles (blue disks) in a two-dimensional periodic channel with temperature difference in the  $y$  direction. The temperature is set to  $T_0$  at  $y = 0$  and  $T_0(1 + \Delta T)$  at  $y = L_y$ . Also, the temperature as a function of  $y$  is described by equation (1). Periodic boundary conditions are imposed in the  $x$  direction and sliding boundary conditions in the  $y$  direction. (b) Sketch of the trajectory for chiral active particle in the free uniform space. The counterclockwise (CCW) particles are positive  $\Omega_i$  and the clockwise (CW) particles are negative  $\Omega_i$ .

moving chiral active particles. Moreover, both particles and obstacles are modeled as soft disks with radius  $r$ . In the two-dimensional channel, periodic boundary conditions and sliding boundary conditions ( $\theta$  is unchanged and the particle will remain adhere and cling to the wall until its orientation points away from it) are imposed in the  $x$  direction (the period  $L_x$ ) and  $y$  direction (the height  $L_y$ ), respectively. The temperature at the lower wall ( $y = 0$ ) and the upper wall ( $y = L_y$ ) are set to  $T_0$  and  $T_0(1 + \Delta T)$ , respectively. The dependence of the temperature on the  $y$  is described as

$$T(y) = T_0 + \delta T \frac{y}{L_y} = T_0 \left( 1 + \Delta T \frac{y}{L_y} \right), \quad (1)$$

where  $T_0$  is the initial temperature of the lower wall.  $\delta T$  and  $\Delta T$  are the absolute temperature difference and the relative temperature difference between the upper wall and the lower wall.

To remove the ambiguity, this equation should refer to the temperature of the particle center of mass. As known, the position and the orientation of a microscopic particle undergoes Brownian diffusion with translational diffusion coefficient and rotational diffusion coefficient, respectively [9, 38].

$$D_T(y) = \mu k_B T_0 \left( 1 + \Delta T \frac{y}{L_y} \right), \quad (2)$$

$$D_\theta(y) = \mu_r k_B T_0 \left( 1 + \Delta T \frac{y}{L_y} \right), \quad (3)$$

where  $k_B$  is the Boltzmann constant,  $\mu$  is the translational mobility and  $\mu_r$  is the rotational mobility. Note that  $\mu$  and  $\mu_r$  are assumed to be independent.

The motion of chiral active particles can be modeled as the combined action of three different processes: random diffusion process, internal self-propelling force and torque [39, 40]. The coordinates of particle  $i$  can be described by the position  $\mathbf{r}_i \equiv (x_i, y_i)$  and it is oriented at an angle  $\theta_i$  of the polar director  $\mathbf{n}$  with the  $x$  axis, i.e.  $\mathbf{n}_i \equiv (\cos \theta_i, \sin \theta_i)$ . The interaction forces acting on particle  $i$  from the other particles and obstacles are defined as  $\mathbf{F}_i = F_i^x \mathbf{e}_x + F_i^y \mathbf{e}_y = \sum \mathbf{F}_{ij}$  and  $\mathbf{G}_i = G_i^x \mathbf{e}_x + G_i^y \mathbf{e}_y = \sum \mathbf{G}_{ij}$ , respectively. For a chiral active particle, due to the torque acting on the particle,  $\theta$  rotates with angular velocity  $\Omega$ . This reorientation of the particle will translate into a rotation around an effective external axis when the self-propulsion speed  $v_0 > 0$ . It is assumed that the torque of the temperature gradient is ignored. In the most general case, the dynamics of active particle  $i$  can be described by the following Langevin equations (assuming overdamped dynamics and neglecting hydrodynamics interactions) [38, 41–43],

$$\frac{dx_i}{dt} = v_0 \cos \theta_i + \mu (F_i^x + G_i^x) + \sqrt{2D_T(y_i)} \xi_i^x(t), \quad (4)$$

$$\frac{dy_i}{dt} = v_0 \sin \theta_i + \mu (F_i^y + G_i^y) + \sqrt{2D_T(y_i)} \xi_i^y(t), \quad (5)$$

$$\frac{d\theta_i}{dt} = \Omega_i + \sqrt{2D_\theta(y_i)} \xi_i^\theta(t), \quad (6)$$

where  $v_0$  is the self-propulsion speed of particles and  $\Omega_i$  is the angular velocity. The  $\Omega_i$  determines the chirality of chiral active particles. We formulate that positive  $\Omega_i$  denotes the counter-clockwise (CCW) particles and negative  $\Omega_i$  denotes the clockwise (CW) particles.  $\xi_i^x(t)$ ,  $\xi_i^y(t)$ , and  $\xi_i^\theta(t)$  represent unit-variance Gaussian white noises with zero mean. For convenience, we scale all variables by the characteristic length  $2r$  and time  $\tau = \frac{1}{\mu k}$ .

The particle-particle interaction force  $\mathbf{F}_{ij}$  and particle-obstacle interaction force  $\mathbf{G}_{ij}$  are modeled as a shot-range repulsion between disks of radius  $r$ ,  $\mathbf{F}_{ij} = k(2r - r_{ij}) \hat{\mathbf{r}}_{ij}$  for  $(r_{ij} < 2r)$  and  $\mathbf{F}_{ij} = 0$  otherwise.  $\mathbf{G}_{ij} = k_1(2r - r_{ij}) \hat{\mathbf{r}}_{ij}$  for  $(r_{ij} < 2r)$  and  $\mathbf{G}_{ij} = 0$  otherwise, with  $k$  and  $k_1$  being the elastic constants.  $r_{ij} = |\mathbf{r}_i - \mathbf{r}_j|$  is the distance between the center of disk  $i$  and disk  $j$  and  $\hat{\mathbf{r}}_{ij} = (\mathbf{r}_i - \mathbf{r}_j) / r_{ij}$ .

In this paper, behaviors of the quantities of interest can be verified by Brownian dynamic simulations performed by integration of the Langevin equations (4)–(6) using the second-order stochastic Runge–Kutta algorithm. The motions of the particles and obstacle arrays are along the  $x$  direction due to the particles and obstacle arrays are confined along the  $y$  direction. So we only calculate the  $x$  direction average velocity. The average velocity of particles and

obstacle arrays along the  $x$  direction in the asymptotic long-time regime can be obtained from these formulas, respectively.

$$V_a = \frac{1}{n_a} \sum_{i=n_o+1}^n \lim_{t \rightarrow \infty} \frac{\langle x_{ai}(t) - x_{ai}(0) \rangle}{t}, \quad (7)$$

$$V_o = \frac{1}{n_o} \sum_{i=1}^{n_o} \lim_{t \rightarrow \infty} \frac{\langle x_{oi}(t) - x_{oi}(0) \rangle}{t}, \quad (8)$$

where  $n = n_o + n_a$  is the total number of disks.

### 3. Results and discussion

In the model, we consider the sliding boundary conditions, which the angle  $\theta$  is unchanged when particles meet the wall. The particle position is initialized within the channel with a uniform random distribution and orientation is random over the interval  $[0, 2\pi]$ . The integration step time ( $dt$ ) was chosen to be smaller than  $10^{-3}$  and the total integration time was more than  $10^5$ . In order to avoid abnormal behaviors in the numerical simulation, we should use a large value of  $k = k_1 (= 100)$  as well as ensure that  $v_0 dt \ll 2r$ . Therefore, particle-obstacle overlaps will decay rapidly and particle cannot move through the obstacles. Unless otherwise noted, our results are under the parameter sets:  $n_a = 64$ ,  $n_o = 36$ ,  $r = 0.5$ ,  $L_x = L_y = 25.0$ ,  $k = k_1 = 100.0$ ,  $k_B = 1.0$ ,  $\mu = 1.0$ , and  $\mu_r = 3.0$ .

We mainly focus on the transport behaviors of the obstacle arrays are driven by chiral active particles. Firstly, we should consider the transport behaviors of chiral active particles. In a uniform free space, chiral active particles move in a circular trajectory (shown in figure 1(b)). However, chiral active particles exhibit different behaviors under asymmetric conditions (such as temperature difference), the circular trajectory will be destroyed as shown in figure 3(b). In figure 3, we present a schematic of the obstacle arrays being driven by the CCW particles. It takes  $t_1$  ( $t_2$ ) for the particles to move along the upper (lower) trajectory from B (A) to A (B). For ease of understanding, we define the time difference between particles moving along the upper part and the lower part of trajectory  $\Delta t = t_1 - t_2$ . The particles on average move to the positive  $x$  direction ( $V_a > 0$ ) for  $\Delta t > 0$  and the negative  $x$  direction ( $V_a < 0$ ) for  $\Delta t < 0$ . But for the obstacle arrays, its behavior is complicated and needs to take more factors into account.

In figure 2(a), we plot the average velocity  $V$  as a function of  $|\Omega|$  for both CCW particles and CW particles. It is shown that the transport direction of CCW particles is exactly opposite to CW particles. This indicates that the transport direction of particles is determined by the chirality of the particles. When  $|\Omega| \rightarrow 0$ , the chirality of particles disappears and the directed transport no longer occurs, thus  $V_a \rightarrow 0$ . When  $|\Omega| \rightarrow \infty$ , the angle  $\theta$  of the particles changes very fast and almost *in situ* rotation, so  $V_a$  tends to zero. Therefore, there is an optimal value of  $|\Omega|$  at which  $V_a$  takes its maximal value. Due to the obstacle arrays are driven by particles, in general, the transport behavior of obstacle arrays is similar to particles and the velocity is numerically smaller than particles. Moreover, figure 2(b) shows The position of the center of mass of the obstacle arrays  $x_c$  versus the computation time  $t$  for different  $\Omega$ . The position of the center of mass  $x_c$  increases linearly with the computation time  $t$ . Obviously, the obstacle arrays are indeed under transportation and the transport direction of CCW particles is completely opposite to that of the CW particles, so we only consider CCW particles ( $\Omega > 0$ ) in the following discussion.

We present a sketch that explains how obstacle arrays are driven by CCW particles in figure 3. Firstly, it is assumed that there are no obstacle arrays. In a uniform free space, chiral

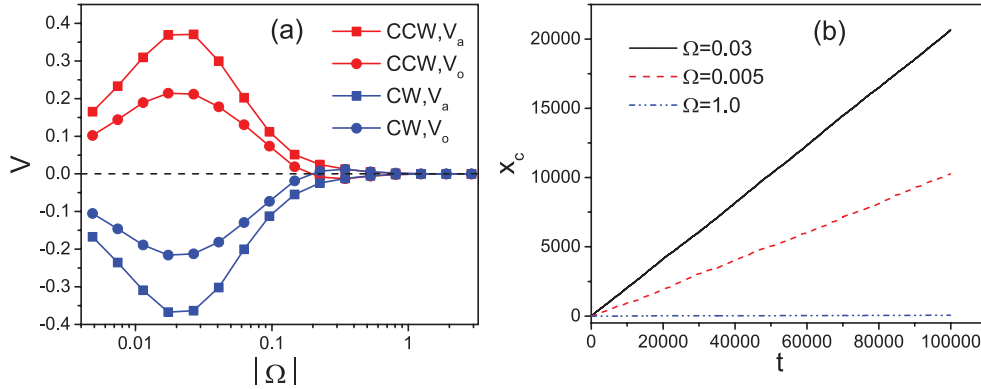


**Figure 2.** (a) Average velocity of chiral active particles and the obstacle arrays  $V$  versus the magnitude of angular velocity  $|\Omega|$  for both CCW particles and CW particles. The other simulation parameter are  $v_0 = 2.0$ ,  $\Delta T = 5.0$  and  $T_0 = 0.003$ . (b) The position of the center of mass of the obstacle arrays  $x_c$  versus the computation time  $t$  for different angular velocity  $\Omega$ . The other simulation parameter are  $v_0 = 2.0$ ,  $\Delta T = 5.0$  and  $T_0 = 0.003$ .

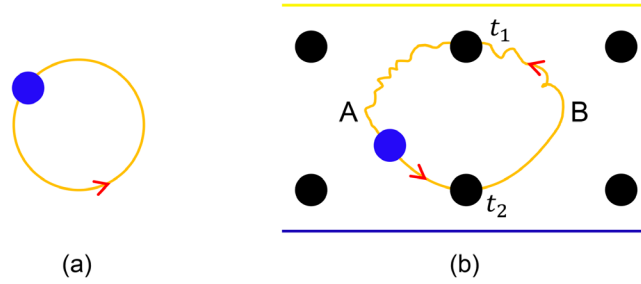


**Figure 3.** The illustrative sketches for motion of CCW particles that are driving obstacle arrays. (a) Circular trajectory of a CCW particle in the free uniform space. (b) Obstacles driven by CCW particles with closed random trajectories in a channel with a temperature difference.

active particles move in a circular trajectory and the radius of the trajectory is approximately  $v_0/|\Omega|$  (shown in figure 3(a)). But in the presence of a temperature difference, the circular trajectory was broken in the channel as shown in figure 3(b) and the trajectory of the chiral active particles close to the upper wall is more random than near the lower wall. Because of the high temperature of the upper wall will destroy the directional transport of the particles. So the upper part of the trajectory is longer and more random than the lower part of the trajectory. The motion time along the lower part (from A to B) is shorter than along the upper part (from B to A) of trajectory, thus CCW particles on average move to the positive  $x$  direction ( $V_a > 0$ ). Similarly, CW particles on average move to the negative  $x$  direction ( $V_a < 0$ ). If there is the array of obstacles in channel, the particles will generate a driving force in the left and right directions of the obstacle: (a) Chiral active particles moving along the upper part of trajectory will collide with the obstacle arrays and drive it to the left. (b) Particles moving along the lower part of trajectory will drive the array of obstacles to the right (see figure 3(b)). The transport direction of obstacle arrays is the result of the above two factors competing with each other. It is worth noting that the temperature of the upper wall is higher than that of the

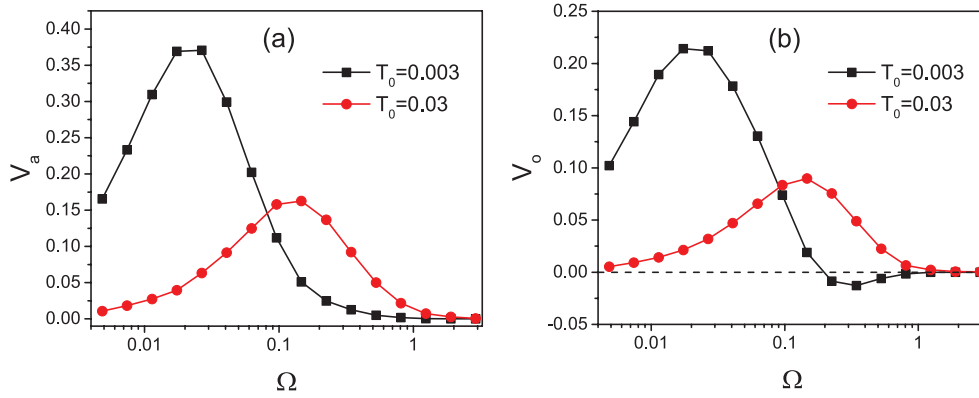


**Figure 4.** (a) Average velocity of chiral active particles  $V_a$  as a function of angular velocity  $\Omega$  for different  $T_0$ . (b) Average velocity of the obstacle arrays  $V_o$  as a function of angular velocity  $\Omega$  for different  $T_0$ . Other simulation parameters are  $v_0 = 2.0$  and  $\Delta T = 5.0$ .

lower wall, so that the thermal motion of the particles near the upper wall is more intense. When the size of the close trajectory ( $v_0/|\Omega|$ ) is large enough, CCW particles will drive the array of obstacles to the right ( $V_o > 0$ ). When  $v_0/|\Omega|$  is small, the difference between the upper part and lower part of the trajectory becomes inconspicuous ( $\Delta t \rightarrow 0$ ). Therefore, the directed transport of CCW particles to the right is attenuated. The obstacle arrays move to the negative  $x$  direction ( $V_o < 0$ ) due to the collisions between the particles near the upper wall are more intense.

Figure 4 shows the dependence of the average velocity of particles  $V_a$  and average velocity of obstacle arrays  $V_o$  on  $\Omega$  for different values of  $T_0$  at  $\Delta T = 5.0$ . Similar to the figure 2, both  $V_a$  and  $V_o$  tend to zero when  $\Omega \rightarrow 0$  or  $\Omega \rightarrow \infty$ , there is an optimal  $\Omega$  at which the amplitude of  $V$  is maximal. However, for different parameters, transport behaviors of obstacle arrays become complex for intermediate  $\Omega$ . When  $T_0$  is large (e.g.  $T_0 = 0.03$ ),  $V_o$  is always positive. When  $T_0$  is small (e.g.  $T_0 = 0.003$ ),  $V_o$  is positive for small  $\Omega$  and negative for large  $\Omega$  as shown in figure 4(b). Current reversal can be observed for small  $T_0$  which is different from particles. This situation can be explained as follows. For large  $T_0$ , the average temperature ( $T_0 + \frac{\delta T}{2} = T_0 (1 + \frac{\Delta T}{2})$ ) is high. Both translational diffusion and rotational diffusion are large, so the directed transport becomes more random. Thus maximal values of  $V_a$  and  $V_o$  become smaller. The position of the peak on the curves shifts to larger  $\Omega$  with the increasing of  $T_0$ . For small  $T_0$  and small  $\Omega$ , the average temperature ( $T_0 (1 + \frac{\Delta T}{2})$ ) is low and the size of the close trajectory ( $v_0/\Omega$ ) is large, the self-propulsion of particles dominates the transport, so maximal values of  $V_a$  and  $V_o$  are more larger and the transport direction is positive. For small  $T_0$  and large  $\Omega$ , the size of the close trajectory ( $v_0/\Omega$ ) decreases, the difference between the upper part and lower part of the trajectory becomes smaller. Thus  $V_o$  reverses its direction ( $V_o < 0$ ).

The average velocity  $V_a$  and  $V_o$  as a function of  $\Omega$  for different  $\Delta T$  at  $T_0 = 0.003$  is shown in figure 5. For different value of  $\Delta T$ ,  $V_a$  is always positive. But  $V_o$  can change its direction and the amplitude of negative  $V_o$  is maximal for intermediate  $\Delta T$ . The position of the positive peak on the curves shifts to large  $\Omega$  with the increasing of  $\Delta T$ . This can be explained as follows. When the value of  $\Omega$  increases, the size of the close trajectory ( $v_0/\Omega$ ) decrease, which can reduce the difference between the upper part and lower part of the trajectory. Current



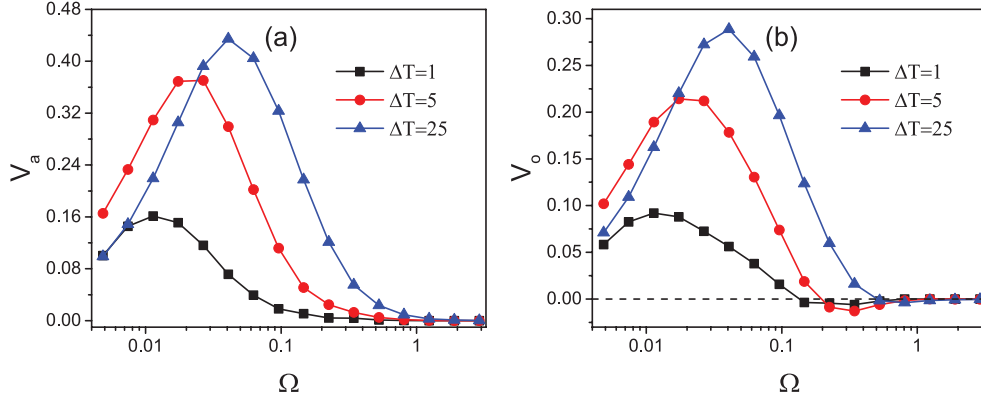


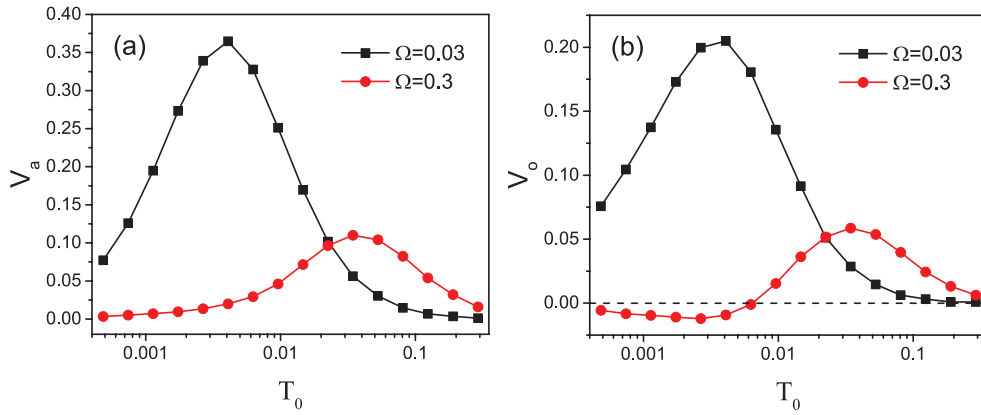
**Figure 5.** (a) The dependence of average velocity of chiral active particles  $V_a$  on angular velocity  $\Omega$  for different  $\Delta T$ . (b) The dependence of average velocity of the obstacle arrays  $V_o$  on angular velocity  $\Omega$  for different  $\Delta T$ . Other simulation parameters are  $v_0 = 2.0$  and  $T_0 = 0.003$ .

reversal occurs for the effect of particles driving the obstacle arrays to the left is stronger than the effect of driving to the right,  $V_o < 0$ . For small  $\Delta T$  (e.g.  $\Delta T = 1.0$ ) and large  $\Omega$ , the temperature difference between the particles moving along the upper half of the trajectory and those moving along the lower half of the trajectory is small. Thus the amplitude of negative  $V_o$  is small. For intermediate  $\Delta T$  (e.g.  $\Delta T = 5.0$ ) and large  $\Omega$ , the effect of particles driving the obstacle arrays to the left increases. Therefore, the amplitude of negative  $V_o$  is large. For large  $\Delta T$  (e.g.  $\Delta T = 25.0$ ) and large  $\Omega$ , the rectified transport of particles is more prominent, the effect of particles driving the obstacle arrays to the right is stronger, so the amplitude of negative  $V_o$  decrease. Similar to figure 2,  $V_a$  and  $V_o$  tend to zero when  $\Omega \rightarrow 0$  or  $\Omega \rightarrow \infty$ .

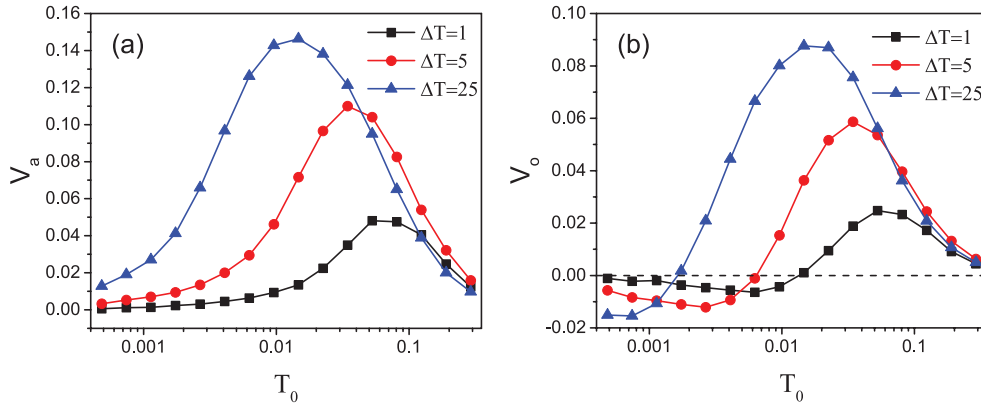
Figure 6 shows the average velocity  $V_a$  and  $V_o$  as a function of  $T_0$  for different  $\Omega$  at  $\Delta T = 5.0$ . It is found that the average velocity  $V_a$  and  $V_o$  are a peaked function of initial temperature  $T_0$ . When  $T_0 \rightarrow 0$ , translational diffusion ( $D_T$ ), rotational diffusion ( $D_\theta$ ) and the average temperature ( $T_0 (1 + \frac{\Delta T}{2})$ ) are almost zero, the directed transport of chiral active particles almost disappears, so  $V_a$  and  $V_o$  tend to zero. When  $T_0 \rightarrow \infty$ , the average temperature ( $T_0 (1 + \frac{\Delta T}{2})$ ) is very high, the directional trajectories of particles become randomized, the self-propulsion of particles can be ignored because of  $D_T$  and  $D_\theta$  are much larger than  $v_0$  and  $\Omega$ , respectively. Thus no directed transport occurs,  $V_a$  and  $V_o$  tends to zero. Therefore, there exist the optimal  $T_0$  at which  $V_a$  and  $V_o$  are maximal. When  $\Omega$  is small,  $V_a$  and  $V_o$  are always positive. For large  $\Omega$ ,  $V_o$  is negative for small  $T_0$  and positive for large  $T_0$ . This can be explained as follows. For small value of  $\Omega$  (e.g.  $\Omega = 0.03$ ), the size of the close trajectory ( $v_0/\Omega$ ) is large, so  $V_a$  and  $V_o$  are positive and the maximal values of  $V_a$  and  $V_o$  are larger (the time difference between particles moving along the upper part and the lower part of trajectory ( $\Delta t$ ) is larger). For large  $\Omega$  (e.g.  $\Omega = 0.3$ ) and small  $T_0$ , similar to the case of the figure 4(b), the effect of particles driving the obstacle arrays to the left is stronger than the effect of driving to the right, thus  $V_o < 0$ . As increasing  $T_0$ , the effect of particles driving the obstacle arrays to the right increases until  $T_0$  is optimal. Therefore,  $V_o$  will reverse its direction to its positive maximal value.

Figure 7 shows the average velocity  $V_a$  and  $V_o$  as a function of  $T_0$  for different  $\Delta T$  at  $\Omega = 0.3$ . Similar to figure 6,  $V_a$  and  $V_o$  tend to zero when  $T_0 \rightarrow 0$  or  $T_0 \rightarrow \infty$ . For all different  $\Delta T$ , we can always change the direction of  $V_o$  by continuously changing  $T_0$ . The position of





**Figure 6.** (a) Average velocity of chiral active particles  $V_a$  versus the initial temperature  $T_0$  of the lower wall for different  $\Omega$ . (b) Average velocity of the obstacle arrays  $V_o$  versus the initial temperature  $T_0$  of the lower wall for different  $\Omega$ . Other simulation parameters are  $v_0 = 2.0$  and  $\Delta T = 5.0$ .



**Figure 7.** (a) Average velocity of chiral active particles  $V_a$  as a function of the initial temperature  $T_0$  of the lower wall for different  $\Delta T$ . (b) Average velocity of the obstacle arrays  $V_o$  as a function of the initial temperature  $T_0$  of the lower wall for different  $\Delta T$ . Other simulation parameters are  $v_0 = 2.0$  and  $\Omega = 0.3$ .

the peak on the curves shifts to small  $T_0$  and the maximal amplitude of negative  $V_o$  increase with the increasing of  $\Delta T$ . Moreover,  $V_o$  is negative for small  $T_0$  (the effect of particles driving the obstacle arrays to the left is stronger). This can be explained as follows. When  $\Delta T$  is large (e.g.  $\Delta T = 25.0$ ), the rectified transport is more prominent, the effect of particles driving the obstacle arrays to the right becomes stronger, so the maximal values of  $V_a$  and  $V_o$  are larger and the critical for the current reversal decreases with the increasing of  $\Delta T$  (see figure 7(b)). Moreover, the temperature is higher close to the upper wall, and the thermal movement of particles moving along the upper part of the trajectory is more intense, thus the maximal amplitude of negative  $V_o$  is larger. As increasing  $T_0$ ,  $V_o$  reverses its direction and finally tends to zero.

The dependence of the average velocity  $V_a$  and  $V_o$  on the temperature difference  $\Delta T$  for different  $\Omega$  is plotted in figure 8 at  $T_0 = 0.003$ . When  $\Delta T \rightarrow 0$ , the channel is uniform, there is no asymmetry, thus rectified transport of chiral active particles disappears,  $V_a$  and  $V_o$  tend

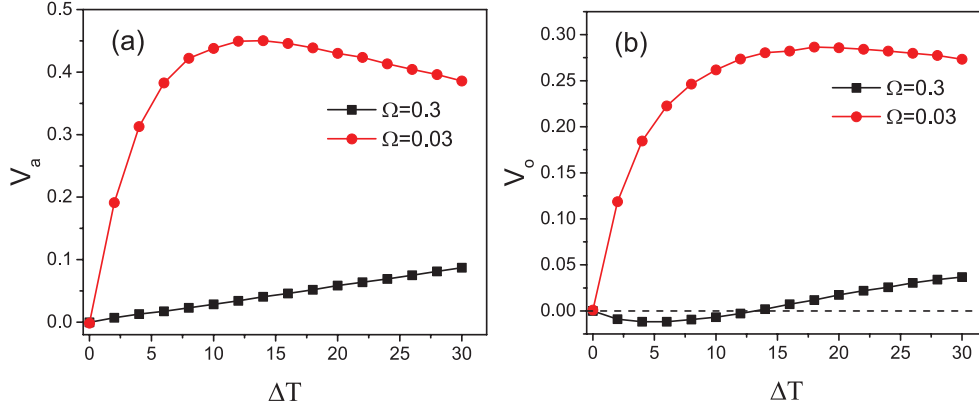


**Figure 8.** (a) Average velocity of chiral active particles  $V_a$  versus the temperature difference  $\Delta T$  for different  $\Omega$ . (b) Average velocity of the obstacle arrays  $V_o$  versus the temperature difference  $\Delta T$  for different  $\Omega$ . Other simulation parameters are  $v_0 = 2.0$  and  $T_0 = 0.003$ .

to zero. When  $\Delta T \rightarrow \infty$ , the average temperature ( $T_0 (1 + \frac{\Delta T}{2})$ ) is very high, the self-propulsion and the chirality of particles can be negligible ( $D_T(y) \gg v_0$  and  $D_\theta(y) \gg \Omega$ ), stochastic motion becomes dominant, so  $V_a$  and  $V_o$  tend to zero. Therefore, there are optimal values of  $\Delta T$  at which  $V_a$  and  $V_o$  take their maximal values. For small  $\Omega$ ,  $V_a$  and  $V_o$  are always positive. For large  $\Omega$ ,  $V_o$  is negative for small  $\Delta T$  and positive for large  $\Delta T$ . This can be explained as follows. Similar to the case of figure 6, when  $\Omega$  is small (e.g.  $\Omega = 0.03$ ), the size of the close trajectory is large, thus  $V_a$  and  $V_o$  are positive. When  $\Omega$  is large (e.g.  $\Omega = 0.3$ ) and  $\Delta T$  is small, the size of the close trajectory is small, the effect of particles driving the obstacle arrays to the left is stronger than the effect of driving to the right, thus  $V_o < 0$ . As increasing  $\Delta T$ , the rectified transport from the temperature difference is more prominent, current reversal occurs,  $V_o$  changes its direction to its positive maximal value as shown in figure 8(b).

The average velocity  $V_a$  and  $V_o$  as a function of the temperature difference  $\Delta T$  for different  $T_0$  is described in figure 9 at  $\Omega = 0.3$ . Similar to the case of figure 8,  $V_a$  and  $V_o$  tend to zero when  $\Delta T \rightarrow 0$  or  $\Delta T \rightarrow \infty$ . For large value of  $T_0$  (e.g.  $T_0 = 0.03$ ),  $V_a$  and  $V_o$  are always positive. When  $T_0$  is small (e.g.  $T_0 = 0.003$ ), as increasing  $\Delta T$  from zero,  $V_o$  first increases to its negative maximal value, then reverses its direction to its positive maximal value, and finally goes to zero. Thus for small  $T_0$ , we can obtain current reversals by changing  $\Delta T$ . Compared with figure 7(b), it is found that, for larger  $\Delta T$ , we need smaller  $T_0$  to achieve current reversals in the case of other simulation parameters remain unchanged.

The average velocity  $V$  as a function of  $v_0$  for chiral active particles and obstacle arrays is shown in figure 10. An increase of the self-propulsion speed  $v_0$  can cause three results: (a) Accelerate particle motion to promote directed transport of particles, (b) enhancing the ability of particles to drive the obstacle arrays and (c) increasing the size of the closed trajectory ( $v_0/\Omega$ ). Thus an increase of  $v_0$  always facilitates the directed transport of particles. However, for small value of  $v_0$  the obstacle arrays will move to the left ( $V_o < 0$ ). Moreover, for large  $v_0$  the average velocity of obstacle arrays will be larger than the average velocity of particles. This can be explained as follows. When  $v_0$  is small, the size of the closed trajectory ( $v_0/\Omega$ ) is small, the effect of particles driving the obstacle arrays to the left is stronger than the effect of driving to the right, thus  $V_o < 0$ . As increasing  $v_0$ , the difference between the upper part and lower part of the trajectory will increase, current reversals occur, so  $V_o > 0$ . For large  $v_0$ , the

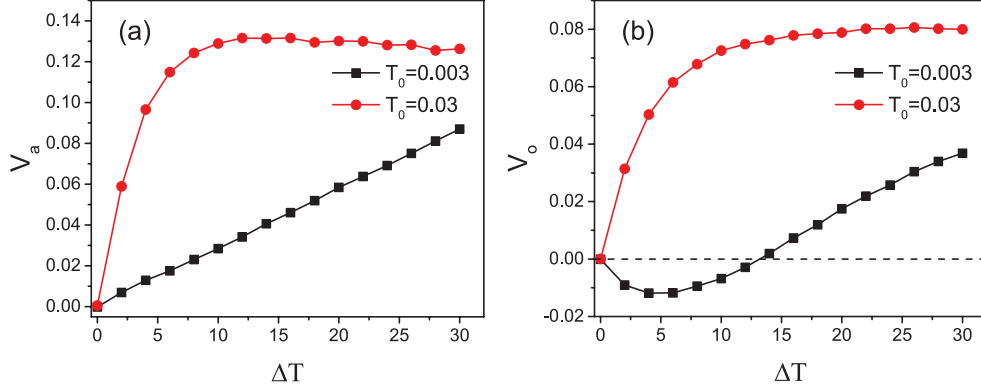


**Figure 9.** (a) Average velocity of chiral active particles  $V_a$  versus the temperature difference  $\Delta T$  for different  $T_0$ . (b) Average velocity of the obstacle arrays  $V_o$  versus the temperature difference  $\Delta T$  for different  $T_0$ . Other simulation parameters are  $v_0 = 2.0$  and  $\Omega = 0.3$ .

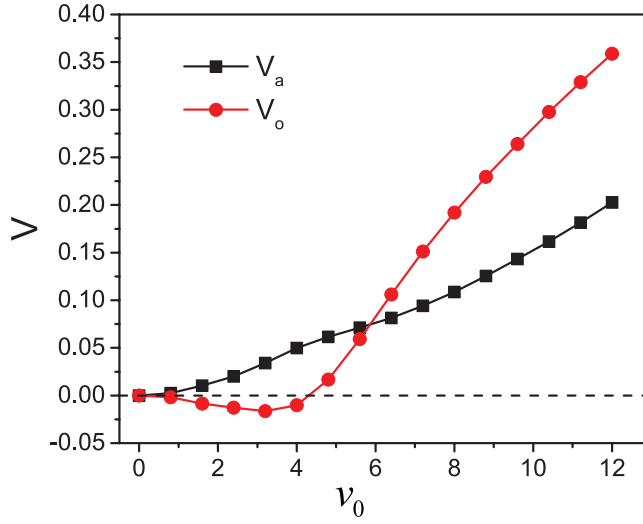


**Figure 10.** The dependence of the average velocity  $V$  on the self-propulsion speed  $v_0$  for chiral active particles ( $V_a$ ) and obstacle arrays ( $V_o$ ). Other simulation parameters are  $\Omega = 0.3$ ,  $\Delta T = 5.0$  and  $T_0 = 0.003$ .

size of the closed trajectory is large, so rectified transport of particles is prominent. However, the array of obstacles is a whole, so the effect of particles driving the obstacle arrays will make  $V_o > V_a$ . Then the average velocity  $V$  increases linearly with self-propulsion speed  $v_0$ .

The dependence of the average velocity  $V$  on the number of chiral active particles  $n_a$  is presented in figure 11. An increase of the numbers of active particles  $n_a$  can cause two results: (a) reducing the mobility of particles and (b) increasing the strength of interactions between particles. Therefore, the increase of the particle number  $n_a$  always prevents the directed motion of particles and  $V_a$  is always positive and its amplitude decreases monotonically with the increase of  $n_a$ . However, the transport behaviors become complex for obstacle arrays. When the value of  $n_a$  is small (e.g.  $n_a < 100$ ), the effect of particles driving the obstacle arrays enhances for increasing  $n_a$ , so  $V_o$  is negative and its amplitude increases to the valley on

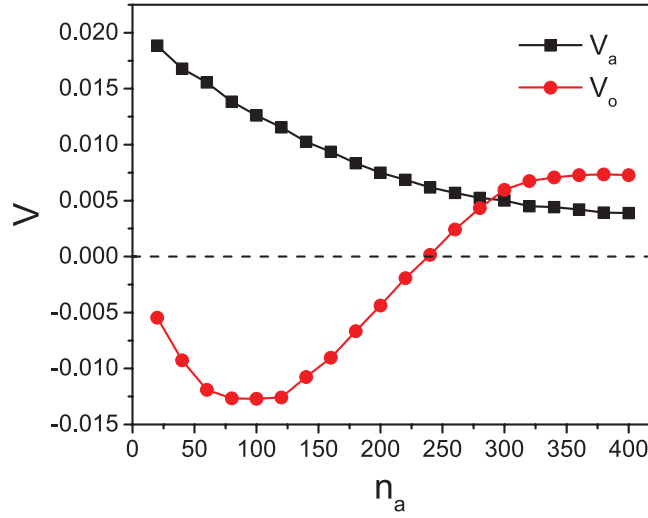


**Figure 11.** Average velocity  $V$  versus the particle number  $n_a$  for chiral active particles ( $V_a$ ) and obstacle arrays ( $V_o$ ). Other simulation parameters are  $v_0 = 2.0$ ,  $\Omega = 0.3$ ,  $\Delta T = 5.0$  and  $T_0 = 0.003$ .

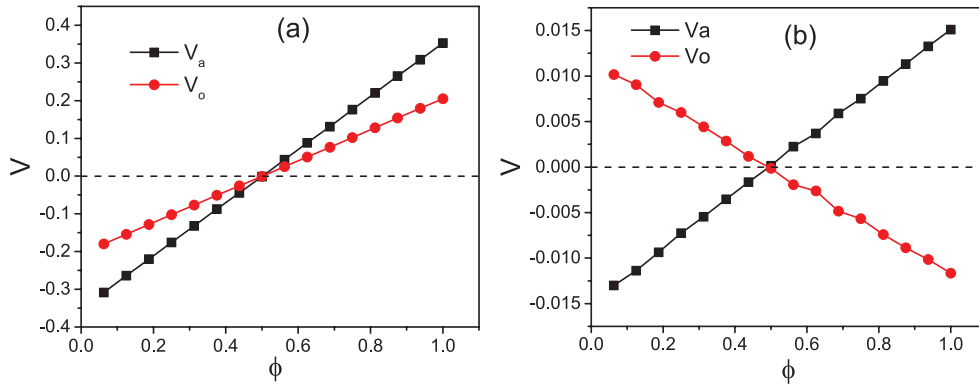


**Figure 12.** Average velocities of chiral active particles ( $V_a$ ) and obstacle arrays ( $V_o$ ) versus the ratios of counterclockwise to clockwise particles  $\phi$  for (a)  $\Omega = 0.03$ , (b)  $\Omega = 0.3$ . Other simulation parameters are  $v_0 = 2.0$ ,  $\Delta T = 5.0$  and  $T_0 = 0.003$ .

the curve. Continue to increase  $n_a$ , the mobility of particles reduces, the channel becomes crowded, thus the amplitude of  $V_o$  gradually decreases, then  $V_o$  changes its direction. When  $n_a$  is large (e.g.  $n_a > 300$ ), particles almost fill the channel, finally  $V_o$  will be greater than  $V_a$ .

The average velocity  $V$  as a function of the ratios of counterclockwise to clockwise particles  $\phi$  is shown in figure 12. The ratios of CCW to CW particles  $\phi$  is described as

$$\phi = \frac{n_{\text{CCW}}}{n_{\text{CW}}}, \quad (9)$$

where  $n_{\text{CCW}}$  and  $n_{\text{CW}}$  are the number of CCW and CW particles, respectively. Obviously, when the number of the CCW particles is the same as the number of CW particles,  $V$  tends to zero. It shows that the transport behavior of CCW and CW particles is completely opposite. According to the previous analysis (see figure 4(b) or 5(b)), when  $\Omega = 0.03$ , the obstacle

arrays move to the positive  $x$  direction. So average velocity of obstacle arrays  $V_o$  goes from negative to positive for increasing  $n_{CCW}$  (see figure 12(a)). Conversely, the obstacle arrays move to the negative  $x$  direction when  $\Omega = 0.3$ .

#### 4. Concluding remarks

In this paper, we have numerically studied the obstacle arrays driven by the moving chiral active particles in a two-dimensional periodic channel with temperature difference. It is found that chiral active particles can drive the obstacle arrays to move along the channel with temperature difference. The transport direction of active particles is completely determined by its chirality and the direction of obstacle arrays depends on the competition of multiple system parameters. The average velocity of chiral active particles is a peaked function of the  $\Omega$  (or  $T_0$ ,  $\Delta T$ ). The average velocity of chiral active particles increases monotonically with the self-propulsion speed and decreases monotonically with the increase of particle number. Moreover, there is an optimal value of  $\Omega$  (or  $T_0$ ,  $\Delta T$ ) at which the amplitude of the average velocity of the obstacle arrays is maximal. However, for small value of  $T_0$ , the average velocity of the obstacle arrays is negative for large  $\Omega$  and small  $\Delta T$ . For large value of  $\Omega$ , the average velocity of the obstacle arrays is negative for small  $T_0$  (or  $\Delta T$ ) and positive for large  $T_0$  (or  $\Delta T$ ). There is a competitive relationship between  $T_0$  and  $\Delta T$  on the transport direction of obstacle arrays. In order to obtain current reversals, a smaller  $T_0$  is required if  $\Delta T$  is larger. The average velocity of the obstacle arrays is negative for small  $v_0$  and then increases monotonically with the increase of  $v_0$ . Therefore, we can control the transport direction of the obstacle arrays by changing the simulation parameters ( $\Omega$ ,  $T_0$ ,  $\Delta T$  and  $v_0$ ). The average velocity of the obstacle arrays is negative for small  $n_a$  and there are a valley and a peak on the curve.

The problem of rectifying motion in non-equilibrium environment is a longstanding issue. Our study suggests the possibility to control transport of the obstacle arrays in asymmetry environments by tuning the parameters of particles in the system. We expect that our results can be generalized to irregular obstacle arrays. In addition, our results should also be relevant to the non-biological chiral active spinners including rotating colloidal systems, granular media and even skyrmions [44–52]. In principle our results could be readily applied to these systems as well.

#### Acknowledgments

This work was supported by the Postdoctoral Science Foundation of China (Grant No. 2019M652931), and the Innovation Project of Graduate School of South China Normal University.

#### ORCID iDs

Yu-Ling He  <https://orcid.org/0000-0002-9765-227X>

#### References

- [1] Marchetti M C, Joanny J F, Ramaswamy S, Liverpool T B, Prost J, Rao M and Simha R A 2013 *Rev. Mod. Phys.* **85** 1143

- [2] Bechinger C, Leonardo R D, Löwen H, Reichhardt C, Volpe G and Volpe G 2016 *Rev. Mod. Phys.* **88** 045006
- [3] Elgeti J, Winkler R G and Gompper G 2015 *Rep. Prog. Phys.* **78** 056601
- [4] Fodor E and Marchetti M C 2018 *Physica A* **504** 106
- [5] Yang X B, Lisa Manning M and Cristina Marchetti M 2014 *Soft Matter* **10** 6477–84
- [6] Romanczuk P, Bär M and Ebeling W 2012 *Eur. Phys. J. Spec. Top.* **202** 1–162
- [7] Menzel A M 2015 *Phys. Rep.* **554** 1
- [8] Zöttl A and Stark H 2012 *Phys. Rev. Lett.* **108** 218104
- [9] Volpe G, Gigan S and Volpe G 2014 *Am. J. Phys.* **82** 659
- [10] Dreyfus R, Baudry J, Roper M L, Fermigier M, Stone H A and Bibette J 2005 *Nature* **437** 862–5
- [11] Nikola N, Solon A P and Kafri Y 2016 *Phys. Rev. Lett.* **117** 098001
- [12] Nagy M, Akos Z, Biro D and Vicsek T 2010 *Nature* **464** 890
- [13] Wioland H, Woodhouse F G, Dunkel J, Kessler J O and Goldstein R E 2013 *Phys. Rev. Lett.* **110** 268102
- [14] Reichhardt C and Olson Reichhardt C J 2013 *Phys. Rev. E* **88** 042306
- [15] Ai B Q, He Y F and Zhong W R 2015 *Soft Matter* **11** 3852
- [16] Aristov M, Eichhorn R and Bechinger C 2013 *Soft Matter* **9** 2525
- [17] Speer D, Eichhorn R and Reimann P 2010 *Phys. Rev. Lett.* **105** 090602
- [18] Meinhardt S, Smiatek J, Eichhorn R and Schmid F 2012 *Phys. Rev. Lett.* **108** 214504
- [19] Chen Q and Ai B Q 2015 *J. Chem. Phys.* **143** 104113
- [20] Ai B Q, Shao Z G and Zhong W R 2018 *Soft Matter* **14** 4388
- [21] Lauga E, DiLuzio W R, Whitesides G M and Stone H A 2006 *Biophys. J.* **90** 400–12
- [22] Di Leonardo R, Dell'Arciprete D, Angelani L and Iebba V 2011 *Phys. Rev. Lett.* **106** 038101
- [23] Denissenko P, Kantsler V, Smith D J and KirkmanBrown J 2012 *Proc. Natl Acad. Sci. USA* **109** 8007–10
- [24] Friedrich B M and Jülicher F 2007 *Proc. Natl Acad. Sci. USA* **104** 13256
- [25] Riedel I H, Kruse K and Howard J 2005 *Science* **309** 300
- [26] Cēbers A 2011 *J. Magn. Magn. Mater.* **323** 279
- [27] Chepizhko O, Altmann E G and Peruani F 2013 *Phys. Rev. Lett.* **110** 238101
- [28] Nourhani A, Crespi V H and Lammert P E 2015 *Phys. Rev. Lett.* **115** 118101
- [29] Kümmel F, Shabestari P, Lozano C, Volpe G and Bechinger C 2015 *Soft Matter* **11** 6187
- [30] Schirmacher W, Fuchs B, Höfling F and Franosch T 2015 *Phys. Rev. Lett.* **115** 240602
- [31] Pinçe E, Velu S K P, Callegari A, Elahi P, Gigan S, Volpe G and Volpe G 2016 *Nat. Commun.* **7** 10907
- [32] Reichhardt C and Reichhardt C J O 2018 *Phys. Rev. E* **97** 052613
- [33] Reichhardt C and Reichhardt C J O 2017 *J. Phys.: Condens. Matter* **30** 015404
- [34] Reichhardt C and Reichhardt C J O 2017 *New J. Phys.* **20** 025002
- [35] Zhu W J, Zhong W R, Xiong J W and Ai B Q 2018 *J. Chem. Phys.* **149** 174906
- [36] Ai B Q, He Y F and Zhong W R 2017 *Phys. Rev. E* **95** 012116
- [37] Ai B Q, He Y F and Zhong W R 2014 *J. Chem. Phys.* **141** 194111
- [38] Ai B Q, Li J J, Li Z Q, Xiong J W and He Y F 2019 *J. Chem. Phys.* **150** 184905
- [39] van Teeffelen S and Löwen H 2008 *Phys. Rev. E* **78** 020101
- [40] Mijalkov M and Volpe G 2013 *Soft Matter* **9** 6376–81
- [41] Levis D and Liebchen B 2018 *J. Phys.: Condens. Matter* **30** 084001
- [42] Liebchen B and Levis D 2017 *Phys. Rev. Lett.* **119** 058002
- [43] Martín-Gómez A, Levis D, Diaz-Guilera A and Pagonabarraga I 2018 *Soft Matter* **14** 2610
- [44] Banerjee D, Souslov A, Abanov A G and Vitelli V 2017 *Nat. Commun.* **8** 1573
- [45] Soni V, Bililign E, Magkiriadou S, Sacanna S, Bartolo D, Shelley M J and Irvine W T M 2018 (arXiv:1812.09990)
- [46] Reichhardt C and Reichhardt C J O 2019 *Phys. Rev. B* **100** 174414
- [47] Reichhardt C and Reichhardt C J O 2019 *Phys. Rev. E* **100** 012604
- [48] van Zuiden B C, Paulose J, Irvine W T M, Bartolo D and Vitelli V 2016 *Proc. Natl Acad. Sci. USA* **113** 12919
- [49] Reichhardt C and Reichhardt C J O 2019 *J. Chem. Phys.* **150** 064905
- [50] Kümmel F, ten Hagen B, Wittkowski R, Buttinoni I, Eichhorn R, Volpe G, Löwen H and Bechinger C 2013 *Phys. Rev. Lett.* **110** 198302
- [51] Han M, Yan J, Granick S and Luijten E 2017 *Proc. Natl Acad. Sci. USA* **114** 7513
- [52] Kokot G, Das S, Winkler R G, Gompper G, Aranson I S and Snezhko A 2017 *Proc. Natl Acad. Sci. USA* **114** 12870